university of groningen / faculty of science and engineering

University of Groningen

Constructing a Synthetic Spectrum of Messier 67 to Test the X-Shooter Spectral Library Simple Stellar Population Models

Master's Thesis

Master of Science in Astronomy
at University of Groningen under the supervision of
Prof. dr. S.C. Trager (Astronomy, University of Groningen)

Sjoerd Koopmans
S3243818

August 20, 2024

Contents

Page

Abstract **3**

1 Introduction **4**

2 Method **6**

2.1 Data 6

2.2 Creating a synthetic spectrum 7

2.2.1 The XSL interpolator 7

2.2.2 Scaling the spectrum 8

2.3 XSL SSP model spectrum 8

2.4 Luminosity functions 8

3 Results **10**

3.1 Comparing the synthetic and XSL model spectra 10

3.2 A restricted model spectrum 12

3.3 The luminosity function 14

4 Discussion **16**

5 Conclusion **19**

Acknowledgements **20**

Appendices **24**

A Pyhton code for creating the synthetic spectrum 24

B Comparison between parsec 1.2S and parsec v2.0 isochrone 25

Abstract

The X-shooter Spectral Library (XSL) Simple Stellar Population (SSP) models (Verro et al., 2022a) are a collection of stellar population models created with an emphasis on the advanced evolutionary stages of stellar evolution. Before these models can be used to study unresolved objects, they need to be tested against resolved systems with well-known key characteristics. To perform a ground-truth test of the XSL SSP models, we create a synthetic spectrum for the open cluster Messier 67 (M67). The synthetic spectrum is generated by interpolating XSL DR3 (Verro et al., 2022b) spectra to the effective temperatures and gravities of M67 stars from Beeson et al. (2024) and summing the individual spectra. We compare the synthetic spectrum to an XSL SSP model spectrum with an age and metallicity similar to that of M67. We find strong agreement between the synthetic spectrum and the XSL model spectrum for the wavelength range of 3500 Å to 6800 Å. For longer wavelengths, however, there is an excess in XSL model flux with the shape of an O-rich giant, reflecting the lack of evolved giants in the underlying M67 Kiel diagram compared with the isochrones used for the XSL SSP models. A comparison with a model restricted to the same temperature and gravity range as our M67 stars shows poor agreement with the synthesized M67 spectrum, with an excess in blue light and a deficit at the red end of the spectrum. The excess in the blue is caused by the underlying isochrone extending to temperatures that are too high compared to the M67 Kiel diagram, and the deficit in the red is due to stochastic variations resulting in more evolved giant stars in the M67 Kiel diagram than predicted by the isochrone. We conclude that the XSL SSP models work well to recreate the spectrum of a population with intermediate age and solar metallicity. However, we find that this comparison has limitations due to our sample of M67 stars, which cannot accurately represent a complete stellar population because of their discrete distribution and the low number of faint dwarfs and evolved giants. Future tests can be performed to assess the XSL SSP models against populations with different parameters, such as older and more metal-poor globular clusters or younger open clusters.

1 Introduction

By studying stellar populations and their evolution in different environments, we gain more understanding of the evolution of galaxies, the conditions under which stars form and the abundances of different elements in the universe. The integrated light of a stellar population is determined by a number of fundamental variables. These include the star formation history (SFH), the stellar initial mass function (IMF), the stellar and gas metallicity and abundance patterns, the total mass in stars and the state and quantity of dust and gas (Conroy, 2013). For populations too distant for individual stars to be discerned, these variables are hidden in the total spectrum of the population. Stellar population synthesis (SPS) is the modelling of the spectral energy distribution (SED) of stellar populations with the aim of extracting these variables from observed SEDs. By comparing models with integrated spectra for real unresolved galaxies we can determine what kind of populations are found in different environments and how galaxies evolve at different cosmic timescales.

With current advancements in wide-field spectroscopic facilities, the quality of spectroscopic information for different environments will increase. Furthermore, with advancement in near-infrared (NIR) instrumentation, the cool evolved stars in stellar populations will be more accessible. SPS models will need to keep up with these current developments. Models can differ in their treatment of virtually all variables responsible for a populations' SED, which can cause large uncertainties between models. Early comparisons between different stellar population models, such as the one by Charlot et al. (1996) uncovered uncertainties between these models and attempted to improve upon them. They concluded that the main source of disagreement is the treatment of stellar evolution, i.e. the underlying isochrones. However, also the spectral library, IMF or the treatment of dust can cause differences between models. Theoretical luminosity functions are also known to cause further uncertainties, mainly due to the different assumptions about mass loss in the red giant branch (RGB) (Schiavon et al., 2002b).

The creation of new SPS models requires only a few ingredients: isochrones that provide stellar evolution information, an IMF and a stellar spectral library. By setting constraints on the age and metallicity of the isochrone, one can create a spectrum for a simple stellar population (SSP) with a single age and metallicity. The stellar library is used to create spectra for all points on the isochrone. The IMF determines the number of stars at each point on the isochrone. The individual spectra are added in the following way (Conroy, 2013):

$$f_{SSP}(t,[Fe/H]) = \int_{m_{\rm low}}^{m_{\rm high}\,(t)} f_*\left(T_{\rm eff}(M), \log g(M) \mid t, [{\rm Fe/H}]\right) \times \Phi(M) dM, \tag{1}$$

where M is the initial stellar mass, Φ(M) is the initial mass function, f_* is a stellar spectrum and f_{ssp} is the resulting spectrum for a given age and metallicity.

Verro et al. (2022a) have created a collection of stellar population models based on the X-shooter Spectral Library (XSL) (Verro et al., 2022b). They were created to improve upon existing models by providing higher resolution and better coverage of the Hertzsprung–Russell (HR) diagram, with an emphasis on the advanced evolutionary stages by including 109 evolved stars beyond the RGB. The XSL models handle the inclusion of these stars differently than previous models. The evolved giants are divided into O-rich static giants, O-rich thermally-pulsing asymptotic giant branch (TP-AGB) stars and C-rich TP-AGB stars. Their spectra are binned by broadband colour and the average spectra is found using empirical relations that dictate where the average spectrum of a star of a certain colour should occur. Evolved stars shape the spectra of stellar populations in the optical–to–NIR (e.g. Mouhcine, Lançon, 2002; Riffel et al., 2015), so with this inclusion the XSL SSP models help to

bridge the gap between the optical and the NIR. The XSL SSP models use the XSL Data Release 3 (DR3) (Verro et al., 2022b) as their spectral library. This library contains 830 spectra of 683 stars, of which a selection of 639 spectra of 534 stars was used. Binaries, supergiants and stars with incomplete data were removed.

New stellar population models require testing against nearby, resolved systems whose key characteristics such as age, metallicity and the IMF are known. This is often done with globular or open clusters since the stars in these clusters all have similar ages and metallicities, thus making the stellar population in the cluster similar to that of the SSPs used in models. Older studies have focused on testing on globular clusters, limiting themselves to ages older than roughly 10 Gyr (e.g. Vazdekis et al., 2001; Maraston et al., 2003). Studies (e.g. Trager et al., 2000; Caldwell et al., 2003) have shown that the lines in the integrated spectrum of early-type galaxies show clear signs of the presence of stars of intermediate age and solar-like metallicity. It is thus of key importance to also test stellar population models against populations with similar age and metallicity.

In this work we test the validity of the XSL SSP models by comparing them to a synthetic spectrum of old open cluster Messier 67 (M67). M67 is an excellent candidate to test the XSL models for a number of different reasons. It is primarily well suited due to its intermediate age and solar metallicity. M67 is one of the oldest known open clusters at an age between 3.5 and 4.0 Gyr (e.g. Sarajedini et al., 2009; Bossini et al., 2019). Open clusters usually only live for a few hundred Myr (Dias et al., 2021) so this makes M67 favourable over other open clusters. Globular clusters are generally much older with ages around 13 Gyr (Valcin et al., 2020). They contain more evolved populations than the intermediate population of M67, making them less desirable to test against the XSL SSP models. The location of M67 is also favourable since it is located nearly 460 pc above the plane of the Milky Way. Open clusters are typically found along the plane of the Milky way making them harder to observe due to dust and gas. The major issue with M67 is that it is too close to create an integrated spectrum with a single measurement, and spectra for all individual stars are not yet available. To circumvent this problem, we create a synthetic spectrum for M67 by adding up spectra for the individual stars created using the XSL interpolator. The aim of this thesis is to create a synthetic spectrum that represents the full integrated spectrum of M67 and to provide a ground-truth test of the XSL SSP models. We compare the XSL model spectrum with the synthetic spectrum and determine to what extent the XSL SSP models still suffer from the limitations of the models that came before.

This work is structured as follows: We present our method of constructing the synthetic spectrum for M67 in Section 2. We compare the synthetic spectrum with the XSL SSP model spectrum in Section 3. We discuss our results and their meaning in Section 4 and we conclude our work in Section 5.

2 Method

The synthetic spectrum for M67 is created in a way similar to a model spectrum for an SSP. We make use of a spectral library, just like in SPS; however, the information on stellar evolution and distribution of stellar mass is provided by a Kiel diagram of M67 as opposed to an isochrone and an IMF. This way we can create an integrated spectrum for M67 without having observed spectra for all the stars in the cluster.

2.1 Data

To create a representative synthetic spectrum of M67, we need spectra for the individual stars in M67. Since observed spectra for all of the individual stars do not exist, we use the XSL interpolator to create synthetic spectra. To feed the interpolator, we need a Kiel diagram with as many stars as possible and that covers all stages of stellar evolution. The Kiel diagram needs to be in $T_{\rm eff}$ and $\log g$ space since the XSL interpolator needs $T_{\rm eff}$, $\log g$ and [Fe/H] as variables to create a spectrum for a star. We start off with a selection of stellar data kindly provided by Kevin Beeson (Beeson et al., 2024). This data is very useful to our goal since Beeson et al. (2024) found more accurate and precise $T_{\rm eff}$ and $\log g$ than those available from GAIA Data Release 3 (DR3) (Vallenari et al., 2023). Their data is a selection of 905 observations of 287 stars based on data from the GAIA DR3. The selection of data is based on a conical search around the cluster centre and by constraining the parallax and the proper motion of the stars. In this work they derive more accurate and precise effective temperatures and surface gravities to find the elemental abundances in open cluster stars. By assuming a normal distribution of stars around the cluster centre and using a joint probability distribution of the cluster size and the location of the cluster centre, they are able to reduce the uncertainties on the distance and absolute magnitude to be able to better fit isochrones to the HR diagram. This allows them to find more accurate and precise $T_{\rm eff}$ and $\log g$. They use these to create a joint photometric probability of $T_{\rm eff}$ and $\log g$. Finally, using this photometric prior, they fit stellar spectra to acquire more precise spectroscopic stellar parameters and abundances.

We further reduce the Beeson et al. (2024) data to better determine the shape of the Kiel diagram. The following constraints were applied:

- a maximum effective temperature of 6800 K for all stars.

For stars with $\log g > 3.5$:

- a microturbulent velocity larger than 0.
- $0 < v_{\sin i} < 15$.
- independent samples > 100 for $T_{\rm eff}$, $\log g$, [Fe/H], v_{mic} and $v_{\sin i}$.

Stars with temperatures over 6800 K are deemed too hot and too far from the main sequence turn off. Stars between 6800 K and 6200 K are considered blue straggler stars. To significantly populate the red giant branch, the other constraints were only applied to stars with $\log g$ larger than 3.5. The constraints on the microturbulent velocity, $v_{\sin i}$ and the number of independent samples are taken from Beeson et al. (2024) and are used since the stars outside these ranges have unreliable abundances. Finally 14 observations are removed by hand since their low surface gravity but high effective temperatures made them unlikely cluster members. We eliminate a total of 267 observations and are left with 629 observations for 201 cluster members. Figure 1 shows the HR diagram of all points and what data points were rejected.

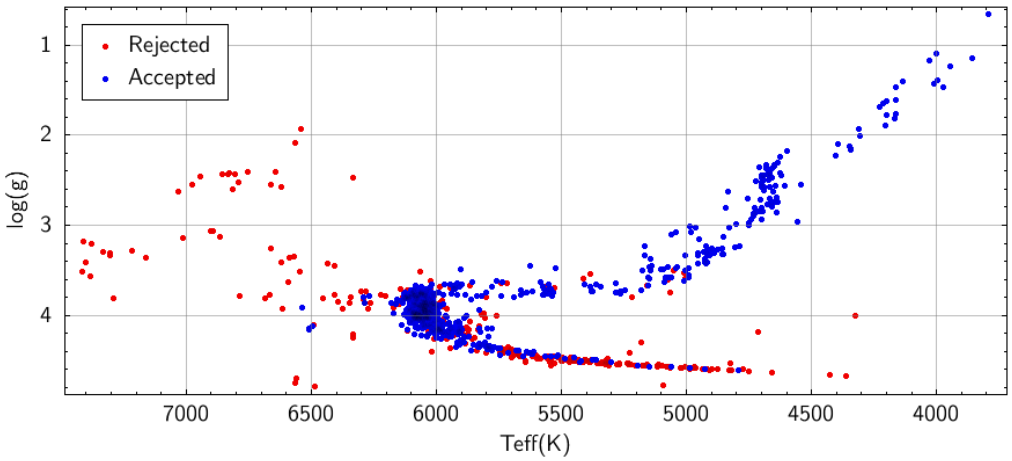

Figure 1: The Kiel diagram of the Beeson et al. (2024) data. Red points are the rejected data points, and blue points are the data used for the synthetic spectrum.

We should note that Beeson et al. (2024) selected their data with a very different goal than ours so their sample primarily contains F, G and K stars. Furthermore, Gaia DR3 does not contain the brightest stars since its instruments were not designed to observe such bright objects (Vallenari et al., 2023).

The luminosity function is an important characteristic of a stellar population. A mismatch in the luminosity function of the model and M67 can cause discrepancies between the two (Schiavon et al., 2002b), especially for giant stars. To accurately represent the integrated spectrum of M67, we average duplicate observations of the same stars in our collection of 629 observations. This is done by taking the average of the $T_{\rm eff}$, $\log g$, [Fe/H] for all observations of each star with more than one observation.

2.2 Creating a synthetic spectrum

To create a total spectrum for M67 we need individual spectra for the stars in M67. To create these spectra, we use the XSL interpolator from Verro et al. (2022a). The interpolator creates a representative stellar spectrum for every star in our Kiel diagram of M67.

2.2.1 The XSL interpolator

Verro et al. (2022a) created an interpolator for the XSL SSP models. This consists of two parts: a global interpolator and a local interpolator. The global interpolator is based on polynomial expansions for each wavelength pixel of the spectrum in powers of the $T_{\rm eff}$, $\log g$ and [Fe/H]. The global interpolator is used for stars between 4500 K and 7000 K. The local interpolator creates a spectrum for a point by looking at the stars in the XSL library that have similar parameters to the point one needs a spectrum for. It then interpolates between the stars closest to this point. The local interpolator is used for starts with $T_{\rm eff} < 4000\,{\rm K}$ or $T_{\rm eff} > 8000\,{\rm K}$. For the region $4000\,{\rm K} < T_{\rm eff} < 4500\,{\rm K}$ and $7000\,{\rm K} < T_{\rm eff} < 8000\,{\rm K}$ a combination of both interpolators is used, where a weight q is used to go smooth from one interpolator to the other:

$$q = \frac{\log(T_{\rm eff}) - \log(T_{\rm lower})}{\log(T_{\rm higher}) - \log(T_{\rm lower})} \tag{2}$$

The global interpolator is not accurate for giant stars with temperatures lower than 4000 K. For stars with lower effective temperatures, a separate interpolator is used. This interpolator uses spectra of static giants, O-rich TP-AGB stars and C-rich TP-AGB stars. For full details on the XSL interpolator we refer to Verro et al. (2022a).

2.2.2 Scaling the spectrum

Not all stars in M67 contribute the same amount of flux to the overall spectrum. We scale the individual spectra to their G-band flux using the GAIA Data Release 3 (Vallenari et al., 2023). We scale the spectrum to the G-band flux by multiplying it by a factor $10^{-0.4M_G}$, where M_G is the absolute magnitude in the Gaia G-band. This absolute magnitude is found using the following relation:

$$M_G = m_G - 5\log(d) - 5 + A_G \tag{3}$$

where m_G is the GAIA DR3 apparent magnitude, d is the distance to the star as found by Beeson et al. (2024) and A_G is the GAIA DR3 extinction in the G-band. For stars with no extinction value we used the mean value of all other stars.

The scaled individual spectra are summed to create a total synthetic spectrum for M67. The Python code for creating the synthetic spectrum is available in Appendix A.

2.3 XSL SSP model spectrum

As described above, the XSL SSP models are based on the X-shooter Spectral Library (Verro et al., 2022b). They use an interpolator to create a model spectrum based on the stellar spectra of the individual stars in the library. Using different isochrones and IMFs, they create spectra for stellar populations with different ages, metallicities and IMFs.

The XSL SSP models have been created for two different sets of isochrones: the PARSEC/COLIBRI (PC) isochrones and the Padova00 isochrones. We have used the PC isochrones[1]. The PARSEC 1.2S models (Bressan et al., 2012; Tang et al., 2014; Chen et al., 2014, 2015) describe stars' evolution from the pre-main sequence to the first thermal pulse in the helium shell after forming the electron-degenerate carbon–oxygen core. The COLIBRI models (Marigo et al., 2013; Rosenfield et al., 2016; Pastorelli et al., 2019, 2020) describe the TP-AGB evolution from the first thermal pulse up to the total loss of the envelope. We used the Kroupa IMF (Kroupa, 2001). This is a double power law with an exponent of $\alpha = 0.35$ for $\frac{m}{M_\odot} < 0.5$ stars and $\alpha = 2.35$ for higher mass stars.

To compare the model spectrum to our synthetic spectrum, we select the spectrum with age and metallicity closest to the age and metallicity of M67. By fitting isochrones to the Kiel diagram of M67, Beeson et al. (2024) found a log age of 9.59 and metallicity of 0.11 dex. We select the model spectrum with log age of 9.6 and metallicity of 0.1 dex.

2.4 Luminosity functions

Schiavon et al. (2002b) showed that differences in the LF can create a discrepancy in the resulting spectra. To check how the LF for our catalogue of stars differs from that of the theoretical models we will create a distribution of the amount of stars at different magnitudes. We use the absolute magnitude

[1] `http://stev.oapd.inaf.it/cgi-bin/Kieldiagram`

as calculated in Eq. 3. For the PC isochrones, the LF is available on the same web interface as the isochrones themselves. It is expressed in the amount of stars, in given magnitude bins over a given magnitude interval. The resulting distribution needs to be scaled with the mass of the cluster since the result is given for one $M_\odot$ of stellar population. For the mass of M67 we used 1400 $M_\odot$ (Hurley et al., 2005). The absolute magnitudes for the stars in our catalogue range from -1.5 to 6, but fall off after magnitude of around 4.2. We assume our selection of stars to be complete up to this magnitude and that it is incomplete for higher magnitudes. To create a good comparison, we used the same interval for the isochrone LF and a binsize of 0.25 mag.

3 Results

We have created a synthetic spectrum for M67. Individual spectra were created for M67 stars by interpolating between XSL DR3 spectra. The total spectrum was made by summing the spectra for individual stars. We now compare this spectrum to a model spectrum with similar age and metallicity to M67.

3.1 Comparing the synthetic and XSL model spectra

Figure 2 shows the resulting synthetic spectrum and the appropriate XSL model spectrum. The spectra are normalised by dividing the flux by their mean for the range of 5250–5750 Å. The two spectra show strong agreement in the wavelength range of 3500–6800 Å. For longer wavelengths there is a excess in flux in the model spectrum.

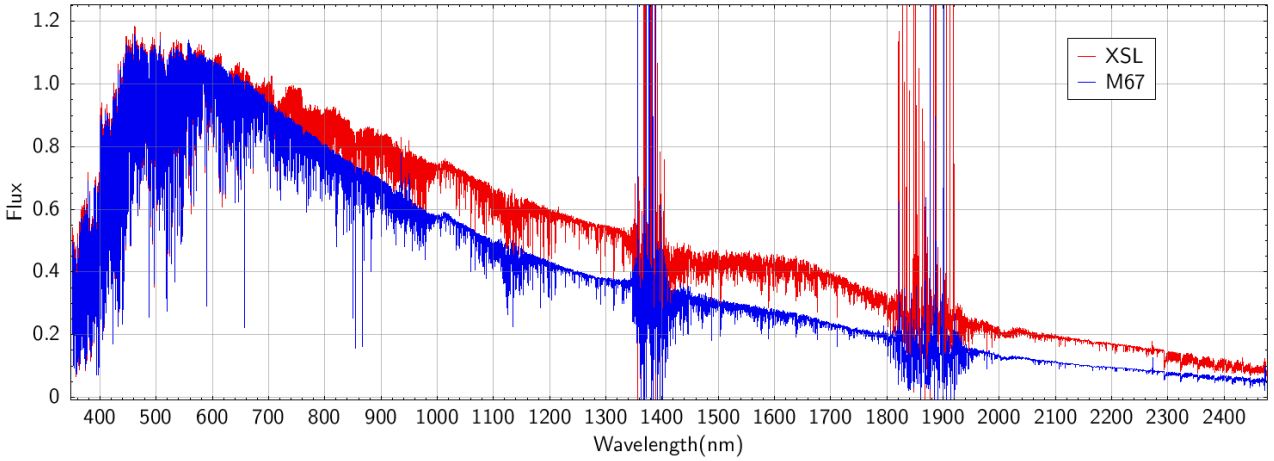

Figure 2: The synthetic spectrum for M67 (blue) and the XSL model spectrum (red) for a stellar population of log age 9.6 and metallicity of 0.1 dex

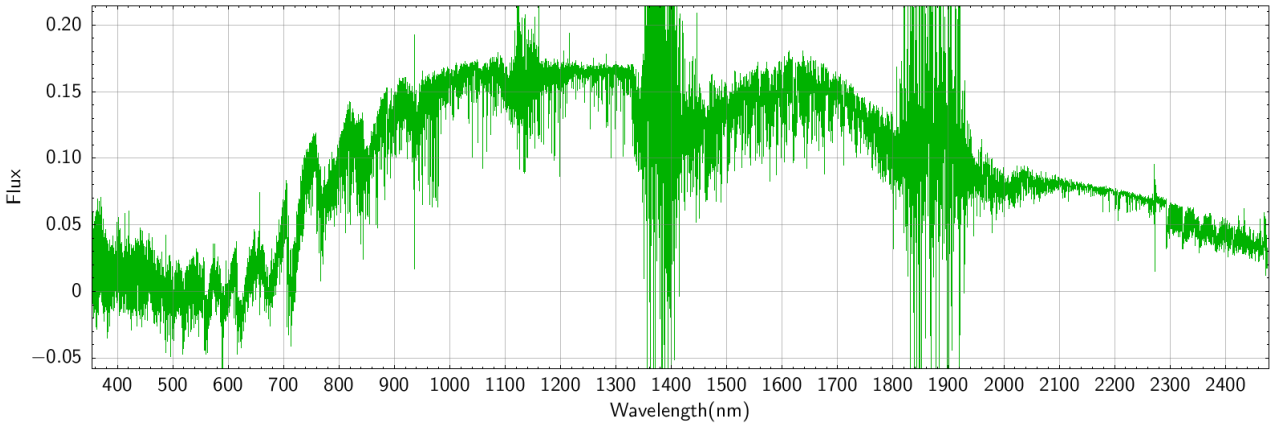

Figure 3: The residual spectrum found by subtracting the synthetic spectrum from the XSL model spectrum

A more insightful way of comparing the spectra is to compute the residual by subtracting the two spectra. Figure 3 shows the XSL model spectrum minus our synthetic spectrum. The residual shows

a clear flux excess in the model spectrum. For the wavelength range of 3500 Å to 6000 Å, the residual is close to zero but with a small excess in the model spectrum. The excess grows larger for longer wavelengths. The excess contains features of the spectrum of an oxygen rich TP-AGB star (O-star). Figure 4 shows the spectrum of O-star X0037 from the XSL DR3 library with similar features.

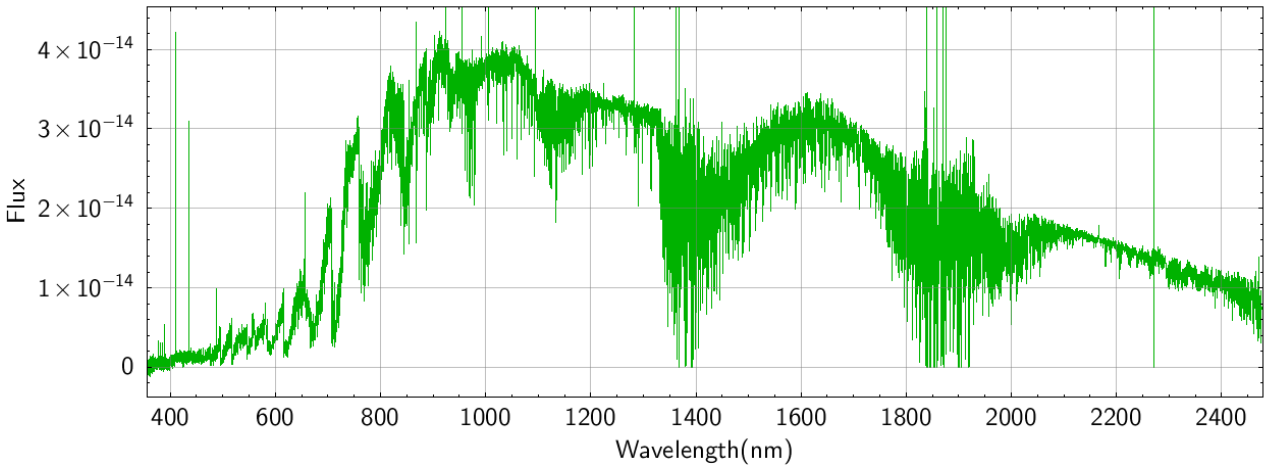

Figure 4: The spectrum of O-star X0037 showing similar features as our residual spectrum

The absorption lines in the residual show a trend where they appear to have an emission-line core in the centre of the absorption line. As an example, Figure 5 shows the Hβ line in the residual spectrum with the ”cored” feature. This feature is due to the difference in spectral line widths for giant stars and dwarf stars. Stars with higher surface gravity have broader lines. Dwarfs have higher surface gravity than giants and thus have broader, shallower lines compared to giants. When we take the residual of the XSL model spectrum minus the synthetic spectrum we see this “cored” pattern in the absorption lines. Therefore, there is a difference in the amount of dwarfs predicted by the XSL models and the amount in our data for M67.

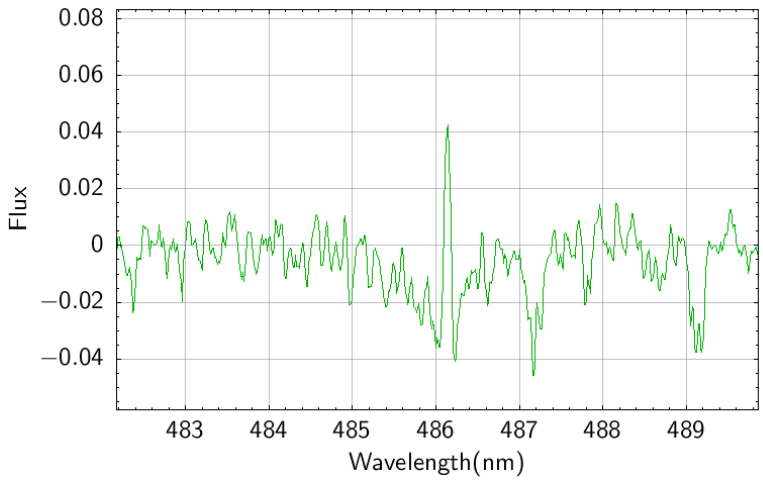

Figure 5: A zoom in on the Hβ absorption line in the residual spectrum at 486 nm, showing the ”cored” profile

3.2 A restricted model spectrum

To account for this difference in stars, we create a new "restricted" model spectrum. We take the PC isochrone for the same age and metallicity as M67, as discussed in Section 2.3, but restrict it to the temperature and gravity range of our Kiel diagram for M67. This the range of $0.65 < \log g < 4.62$ and $T_{\text{eff}} > 3793$. Figure 6 shows the Kiel diagram for our M67 stars and the points on the isochrone included in the restricted model. We run these remaining points on the isochrone through the interpolator, creating a spectrum for every point on the isochrone. We sum the spectra weighted by a Kroupa IMF to create the new restricted model spectrum, which is shown in Figure 7.

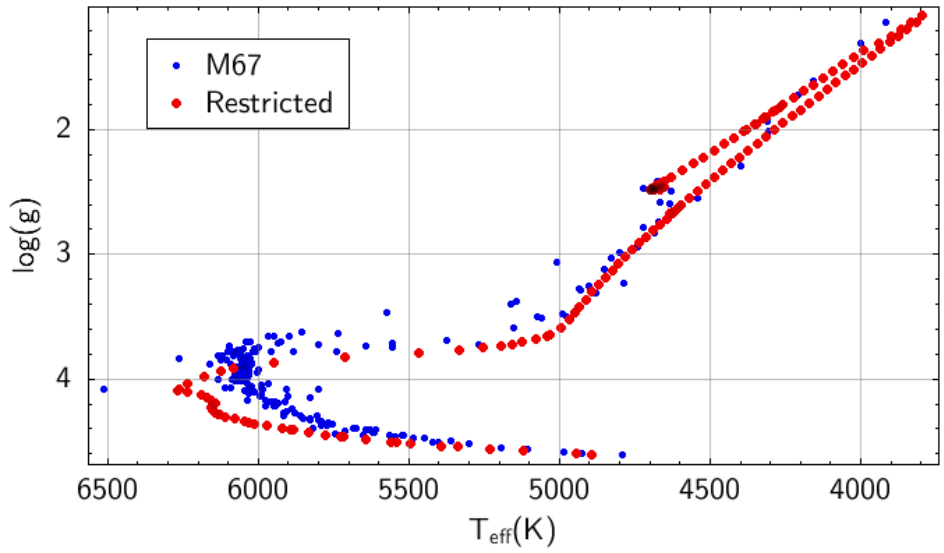

Figure 6: Kiel diagram of the M67 stars (blue) and the restricted isochrone (red).

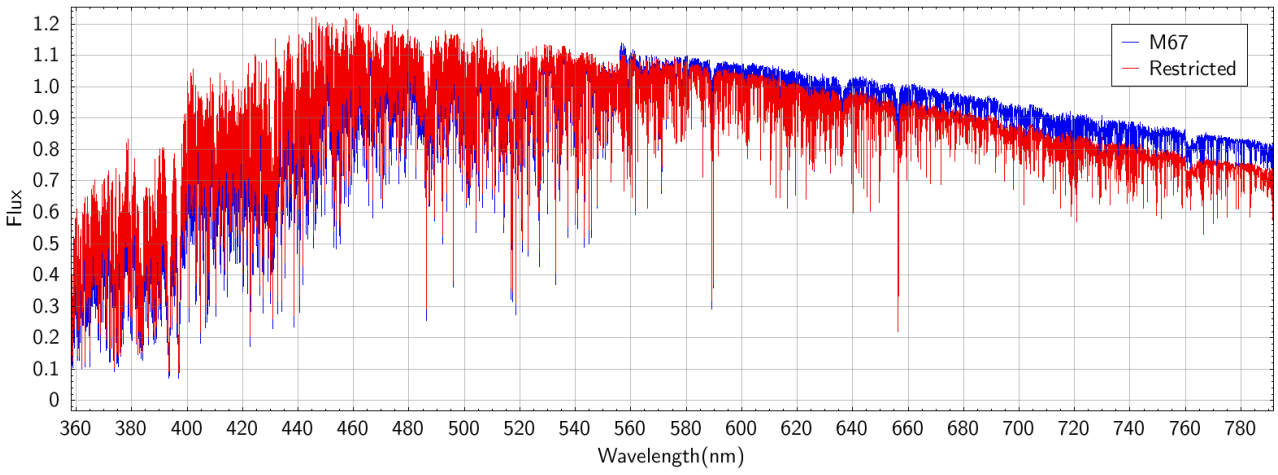

Figure 7: The synthetic spectrum for M67 (blue) and the spectrum found using the restricted isochrone (red) for the wavelength range of 350 to 800 nm.

The restricted model shows worse agreement with the synthetic spectrum than the (full) XSL SSP model spectrum. Where the model spectrum showed good agreement in the blue end and an excess of light in the red end, the restricted spectrum shows an excess in the blue end and a deficit in the

red end of the spectrum. Figure 8 shows the residual when subtracting the restricted model spectrum from our synthetic spectrum. Here we also see the excess in red light from the synthetic spectrum and the deficit in blue light when compared to the restricted model. When we examine the Kiel diagram for both spectra in Figure 6, it is apparent that the isochrone extends to higher temperatures than the M67 stars, resulting in more flux in the blue end. The deficit in the red end of the spectrum points to the isochrone containing fewer of the more evolved red stars than the selection of M67 stars. To confirm this we look at the number of stars for different temperatures. This is shown in Figure 9. It shows that the restricted model has a higher maximum temperature of around 6300 K where the M67 stars only go up to roughly 6200 K, not including the two blue stragglers. It also shows that at this scale, the restricted model has roughly 3 low-temperature stars below 4800 K where the selection of M67 stars has 23 stars.

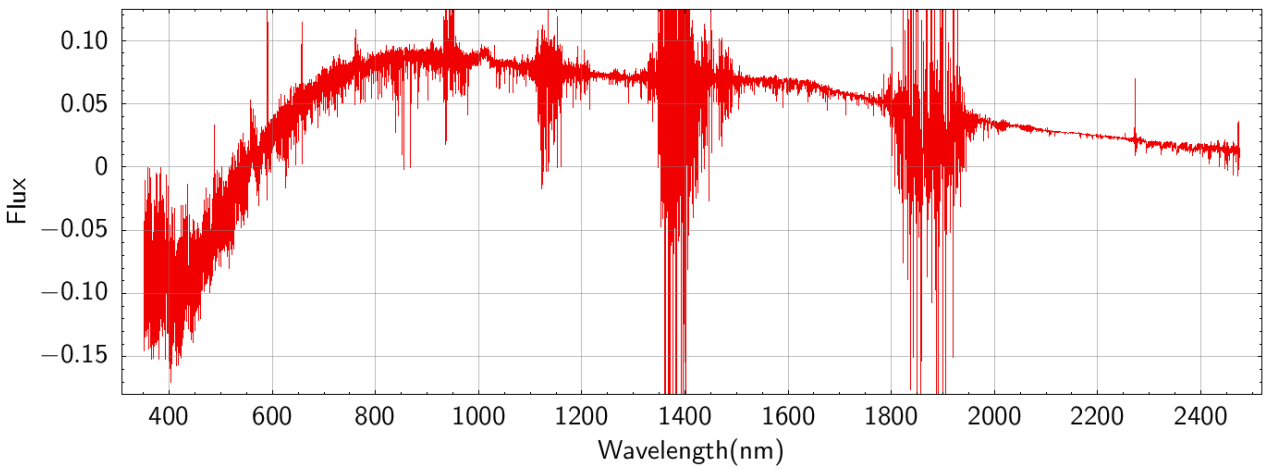

Figure 8: The residual spectrum found by subtracting the restricted spectrum from the synthetic spectrum

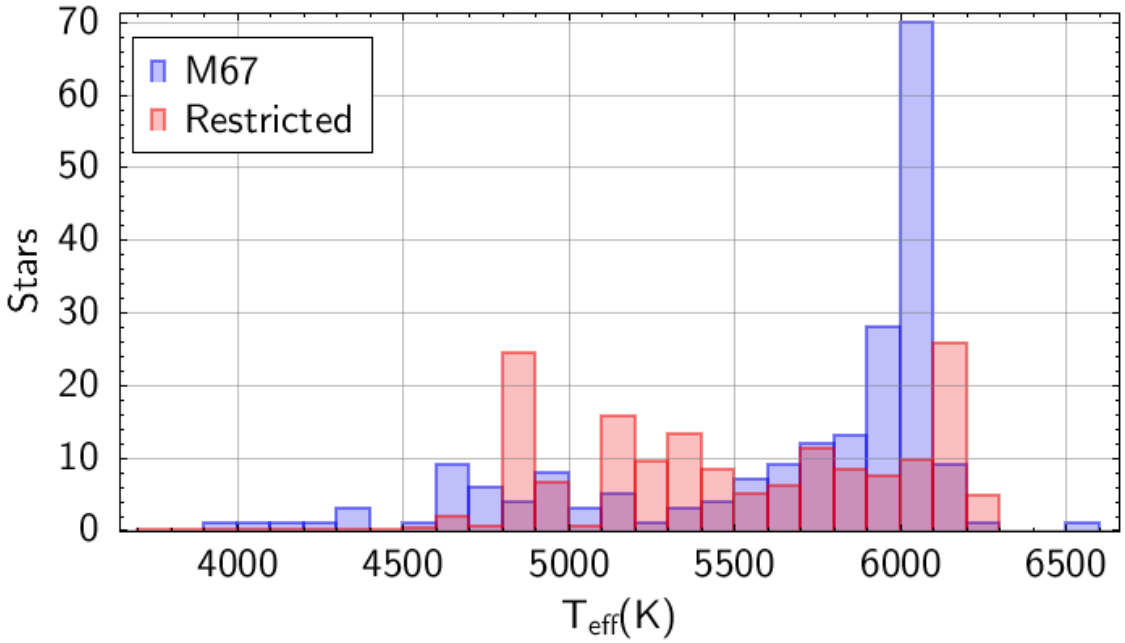

Figure 9: The number of stars at different temperatures for the selection M67 stars (blue) and the restricted isochrone model (red). The number of stars used in the restricted isochrone model have been scaled to the same number of stars as in our collection of M67 stars.

3.3 The luminosity function

As mentioned in Section 1, Schiavon et al. (2002b) showed that the luminosity functions (LF) underlying the isochrones can also can cause discrepancies between different models. When the LFs differ too much, this will cause uncertainties in age estimation and spectral contribution from more evolved stars. Figure 10 shows the LF for our synthetic spectrum, the XSL model spectrum and for our restricted model. All functions have been cut off at a magnitude of $M_G = 4.2$ since the LF for the data from Beeson et al. (2024) falls of rapidly for higher magnitudes. We assume our selection of stars to be complete for stars with $M_G < 4.2$. The LFs for the XSL models and our restricted model have been scaled to the same amount of stars as our M67 LF. We see from this figure that the XSL model overestimates the number of faint dwarfs in M67. On the bright end we see that our list of stars contains more bright giants than predicted by the XSL model. The luminosity function for the restricted model shows that even when we restrict the model to the same temperature and gravity range, the isochrone overestimates the amount of (hot) dwarfs in M67.

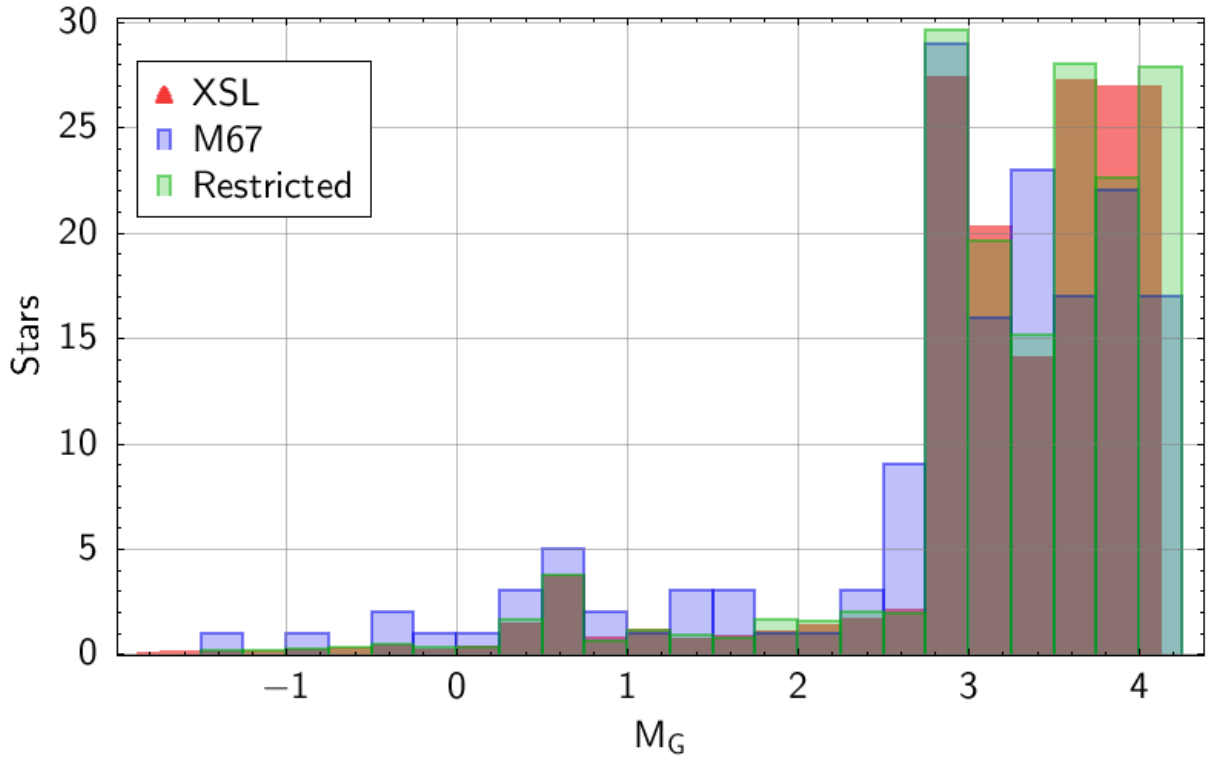

Figure 10: The luminosity functions for our synthetic spectrum (blue), the XSL model spectrum (red) and the restricted isochrone spectrum (green). A faint magnitude limit of $M_G < 4.2$ was imposed, as we assume our selection of stars of M67 complete down to this magnitude. The LF for the two models were scaled to the same number of stars as the M67 LF.

4 Discussion

We have created a synthetic spectrum for M67 to test the validity of the XSL SSP models, comparing it with an XSL model spectrum of similar age and metallicity. We find good agreement between the two spectra for the wavelength range 3500–6800 Å. For longer wavelengths there is an excess of XSL model flux, and the residual between the two spectra shows features of the spectrum of an O-star star. A detailed examination shows a difference in the contribution from dwarfs and giants for the two different spectra. When we create a model spectrum restricted to the same temperature and gravity range as our Kiel diagram of M67, we find worse agreement due to differences in distribution of stars over different temperatures. The luminosity functions for our models support our earlier conclusions. In this section we discuss our results.

The presence of O-rich giant star features in the residual spectrum points to the XSL model overestimating the presence of such stars in a stellar population like M67. The COLIBRI tracks by Marigo et al. (2017) used in creating the XSL SSP models contain evolutionary tracks for TP-AGB stars including O-rich giant stars. From the residual we can conclude that the contribution from such stars is also included in the model for a population with the age and metallicity of M67. Our sample of stars for M67 contains no O-rich giant stars. This can be due to the the fact that M67 does not contain any O-rich giant stars or they were cut from our sample by the selection of stars as discussed in Section 2.1.

Using the PC-isochrone for a population with log age of 9.59 and a metallicity of 0.1 dex in combination with a Kroupa IMF, we can calculate the odds of encountering an O-rich giant star in a population with the size of M67. The IMF predicts 1.2104×10^{-5} stars in the TP-AGB phase of the isochrone for a population of 1 $M_{\odot}$. In the XSL SSP models, the TP-AGB phase is modelled using O-rich giant stars until the carbon over oxygen ratio becomes one. However, none of the stars on the isochrone reach a C/O ratio of 1 so all TP-AGB stars can be considered O-rich giant stars. So when we scale the 1.2104×10^{-5} O-stars to the mass of M67 of 1400 $M_{\odot}$ we find 0.0169 O-rich TP-AGB stars. This means only 1 in 59 stellar populations with the age, metallicity and mass of M67 will host an O-rich TP-AGB star.

The residual spectrum of the XSL model and our synthetic spectrum shows features caused by a difference in the contribution from dwarfs and giant stars. As discussed in Section 3, dwarfs have higher surface gravities causing them to have broader absorption features, while giants have lower surface gravities and thus have more narrow absorption lines. The XSL model spectrum overestimates the number of dwarfs in M67, resulting in more narrow and deeper absorption lines. When we subtract the synthetic spectrum it results in the "cored" (emission-like) features as shown in Figure 5. A possible explanation is that our collection of stars for M67 is incomplete. The fainter stars in M67 are not included in the survey by Beeson et al. (2024) or did not meet the constraints set for this thesis. The luminosity function for our synthetic spectrum contains virtually no stars fainter than $M_G > 4.2$ where both the XSL model and restricted model extend to fainter magnitudes.

Both these results point to our selection of stars not being able to accurately populate the IMF of a representative stellar population. M67 is too small to contain evolved stars such as O-rich TP-AGB stars. The isochrones used by the XSL SSP models do include these stars in their evolutionary tracks. Furthermore, our selection of stars is missing the fainter stars that are included in the model spectra. An observed spectrum for the full cluster could provide a better comparison since this would include the fainter stars that are left out in this work. However M67 is too close for such a spectrum to be created with current instruments. Another solution could be to empirically correct the synthetic spectrum by manually adding stars that are missing. By creating a better match between the LFs, the

synthetic spectrum will more accurately represent a stellar population as used in the models (Schiavon et al., 2002a).

When we compare our synthetic spectrum with a model spectrum that has been restricted to the same temperature and gravity range as our M67 stars, we encounter other issues. In Figure 6 we observe that the isochrone overestimates the maximum temperature of the population of stars and contains too few evolved red stars. The overestimation of blue stars is due to the Main Sequence Turn Off (MSTO) for the isochrone lying at a higher temperature than the MSTO of our collection of M67 stars. The location of the MSTO is linked to the age of a stellar population. Different isochrones have been known to return different ages for the same object when used in SPS (Schiavon et al., 2002b). We note that Beeson et al. (2024) show the same difference in the MSTO between their Kiel diagram and the PC isochrone in Figure 9 of their paper. Nguyen et al. (2022) make a comparison between the parsec v1.2S isochrone and the newer parsec v2.0 version when attempting to fit the Kiel diagram of M67. They find the v2.0 isochrone fits better in M_G and $BP - RP$ space than the v1.2S version, however when when we recreate the comparison in $T_{\rm eff}$ and $\log g$ space we find the MSTO for the parsec v2.0 isochrone extends to even higher temperatures than the v1.2S version does. The comparison is shown in appendix B. There clearly is an existing issue with the isochrones when modelling the stars around the MSTO. We leave this issue to be solved by future work.

Furthermore, M67 has a finite number of stars, so stochastic variations from the continuous distribution assumed by the isochrones used by the XSL SSP models are to be expected (Fouesneau, Lançon, 2010). Most of the light of a population such as M67 is provided by a few bright stars so fluctuations in the presence of these bright stars can easily cause differences in the total spectrum.

In Section 2.1 we apply a number of constraints on our data set. We do not apply these constraints to stars with $\log g < 3.5$. Our aim here is to keep a well populated red giant branch. Making this distinction when constraining our stars may have caused a bias in the number of evolved stars in our sample. Especially when comparing the synthetic spectrum with the restricted model, we observe a surplus of flux for longer wavelengths, as seen in Figure 7. This can be the consequence of bias in the number of bright and red stars in our sample of M67 stars. Additionally, when creating the synthetic spectrum, the interpolator for giant stars with temperatures lower than 4000 K did not work predictably, so the two coolest data points in Figure 1 have not been included. This was also an issue when creating the restricted spectrum. The contribution from the coolest stars in the truncated isochrone was not included what may also have contributed to the deficit in the red end of the spectrum in Figure 7.

M67 is also home to a number of blue straggler stars. These are cluster stars with higher temperatures than is to be expected in their population making the blue stragglers appear younger than the other stars. Our list of stars contains 2 blue stragglers. They are visible as the two hottest stars in Figure 6. Blue stragglers are not included in the PC isochrones, but blue stragglers are known to have very low contribution to the integrated light of a population (Schiavon et al., 2002b). We observed no significant difference when including or eliminating the blue stragglers, so they are included and we have not further investigated their influence.

This work suffers from a number of limitations. As discussed before, our selection of stars for M67 contains too few faint dwarfs and has no contribution from evolved stars such as O-rich TP-AGB stars. As also mentioned, a potential solution is to empirically improve the collection of stars by adding more stars to the areas where the LF for our stars differs from the model LF. However this was beyond the scope of this thesis. Finally, future research that builds upon this work should ensure that the interpolator for cool evolved stars with $T_{\rm eff}$ lower than 4000 K is working predictably. The inclusion of these stars is what sets the XSL SSP models apart from other models and other tests of

their validity should include the evolved stars in the same way.

By testing the XSL SSP models against a synthetic spectrum of M67, we have really only tested a single spectrum in the collection of spectra in the XSL SSP models. Further testing should be done using clusters with different characteristics than M67. A possible candidate for further testing is globular cluster 47 Tucanae (47 Tuc). 47 Tuc is a good candidate since it is well-studied and close enough for the individual stars to be measured. Full integrated observed spectra are also available (e.g. Schiavon et al., 2005). This means the XSL model can be tested against a synthetic spectrum and an observed spectrum. A disadvantage of using 47 Tuc could be the uncertainty in its age (Brogaard et al., 2017). Testing against populations younger than M67 such as younger open clusters would also be a good opportunity to test the XSL models against even more different stellar populations.

5 Conclusion

We have created a synthetic spectrum for M67 in order to test the XSL SSP models. The goal was to determine to what extend the XSL SSP model are able to reproduce the spectrum of a real stellar population and what issues are still embedded in the models. After our comparison we can make the following conclusions:

1. The model spectrum shows an overall strong agreement with the synthetic spectrum. For longer wavelengths the XSL model overestimates the contribution from more evolved stars.

2. The selection of stars for M67 in this work is too small to accurately represent a continuous stellar population as used in the XSL SSP models. The synthetic spectrum contains no faint dwarfs causing differences in absorption features compared to the XSL model spectrum.

3. Differences in the description of stellar evolution around the MSTO by the isochrones compared to the observed Kiel diagram can cause large differences in the integrated light of a stellar population.

4. The discrete and finite distribution of stars in M67 causes differences when its spectrum is compared to that of a continuous population. A few bright stars are responsible for most of its integrated light so stochastic variations make a fair comparison with a continuous population difficult.

The XSL SSP models work well in recreating the integrated spectrum for a stellar population of intermediate age and solar metallicity. The comparison in this work suffers from a number of limitations such as a limited sample of M67 stars and no contribution from the most evolved stars due to our interpolator not working well for these stars. Future tests with stellar populations with different characteristics such as 47 Tuc or younger open clusters can be performed to further test the accuracy and versatility of the XSL SSP models. The models should give promising results when they are ready to be compared to unresolved galactic spectra, especially since these will not suffer from part of the limitations in this work.

Acknowledgments

This research made use of the PARSEC-COLIBRI stellar tracks and isochrones by use of their web interface, hosted by Léo Girardi.

This research used data from Beeson et al. (2024), kindly provided by Kevin Beeson.

This research used the XSL SSP models created by Kristiina Verro. The XSL DR3 and the XSL interpolator created by Kristiina form the backbone of this research and it would not have been possible without it.

I would like to thank Scott Trager for his help throughout this entire project. As my supervisor, he was always patient and always made time in his busy schedule to help me move forward. This project would not have been remotely possible without him.

Bibliography

Beeson Kevin L, Kos Janez, Grijs Richard de, Martell Sarah L, Buder Sven, Traven Gregor, Lewis Geraint F, Zafar Tayyaba, Bland-Hawthorn Joss, Freeman Ken C, others . The GALAH survey: elemental abundances in open clusters using joint effective temperature and surface gravity photometric priors // Monthly Notices of the Royal Astronomical Society. 2024. 529, 3. 2483–2526.

Bossini D, Vallenari Antonella, Bragaglia Angela, Cantat-Gaudin T, Sordo ROSANNA, Balaguer-Núñez L, Jordi C, Moitinho A, Soubiran C, Casamiquela L, others . Age determination for 269 Gaia DR2 open clusters // Astronomy & Astrophysics. 2019. 623. A108.

Bressan Alessandro, Marigo Paola, Girardi Léo, Salasnich Bernardo, Dal Cero Claudia, Rubele Stefano, Nanni Ambra. PARSEC: stellar tracks and isochrones with the PAdova and TRieste Stellar Evolution Code // Monthly Notices of the Royal Astronomical Society. 2012. 427, 1. 127–145.

Brogaard K, VandenBerg Don A, Bedin LR, Milone AP, Thygesen A, Grundahl Frank. The age of 47 Tuc from self-consistent isochrone fits to colour–magnitude diagrams and the eclipsing member V69 // Monthly Notices of the Royal Astronomical Society. 2017. 468, 1. 645–661.

Caldwell Nelson, Rose James A, Concannon Kristi Dendy. Star formation histories of early-type galaxies. I. Higher order Balmer lines as age indicators // The Astronomical Journal. 2003. 125, 6. 2891.

Charlot Stephane, Worthey Guy, Bressan Alessandro. Uncertainties in the modeling of old stellar populations // Astrophysical Journal v. 457, p. 625. 1996. 457. 625.

Chen Yang, Bressan Alessandro, Girardi Léo, Marigo Paola, Kong Xu, Lanza Antonio. PARSEC evolutionary tracks of massive stars up to 350 M at metallicities 0.0001 Z 0.04 // Monthly Notices of the Royal Astronomical Society. 2015. 452, 1. 1068–1080.

Chen Yang, Girardi Léo, Bressan Alessandro, Marigo Paola, Barbieri Mauro, Kong Xu. Improving PARSEC models for very low mass stars // Monthly Notices of the Royal Astronomical Society. 2014. 444, 3. 2525–2543.

Conroy Charlie. Modeling the panchromatic spectral energy distributions of galaxies // Annual Review of Astronomy and Astrophysics. 2013. 51. 393–455.

Dias Wilton S, Monteiro Héktor, Moitinho Aandré, Lépine Jácques RD, Carraro Giovanni, Paunzen Ernst, Alessi Bruno, Villela Lázaro. Updated parameters of 1743 open clusters based on Gaia DR2 // Monthly Notices of the Royal Astronomical Society. 2021. 504, 1. 356–371.

Fouesneau Morgan, Lançon Ariane. Accounting for stochastic fluctuations when analysing the integrated light of star clusters-I. First systematics // Astronomy & Astrophysics. 2010. 521. A22.

Hurley Jarrod R, Pols Onno R, Aarseth Sverre J, Tout Christopher A. A complete N-body model of the old open cluster M67 // Monthly Notices of the Royal Astronomical Society. 2005. 363, 1. 293–314.

Kroupa Pavel. On the variation of the initial mass function // Monthly Notices of the Royal Astronomical Society. 2001. 322, 2. 231–246.

Maraston Claudia, Greggio L, Renzini A, Ortolani S, Saglia RP, Puzia TH, Kissler-Patig M. Integrated spectroscopy of bulge globular clusters and fields-II. Implications for population synthesis models and elliptical galaxies // Astronomy & Astrophysics. 2003. 400, 3. 823–840.

Marigo Paola, Bressan Alessandro, Nanni Ambra, Girardi Léo, Pumo Maria Letizia. Evolution of thermally pulsing asymptotic giant branch stars–I. The COLIBRI code // Monthly Notices of the Royal Astronomical Society. 2013. 434, 1. 488–526.

Marigo Paola, Girardi Léo, Bressan Alessandro, Rosenfield Philip, Aringer Bernhard, Chen Yang, Dussin Marco, Nanni Ambra, Pastorelli Giada, Rodrigues Thaise S, others . A new generation of PARSEC-COLIBRI stellar isochrones including the TP-AGB phase // The Astrophysical Journal. 2017. 835, 1. 77.

Mouhcine M, Lançon A. The modelling of intermediate-age stellar populations-I. Near-infrared properties // Astronomy & Astrophysics. 2002. 393, 1. 149–166.

Nguyen CT, Costa G, Girardi L, Volpato G, Bressan A, Chen Y, Marigo P, Fu X, Goudfrooij P. PARSEC V2. 0: Stellar tracks and isochrones of low-and intermediate-mass stars with rotation // Astronomy & Astrophysics. 2022. 665. A126.

Pastorelli Giada, Marigo Paola, Girardi Léo, Aringer Bernhard, Chen Yang, Rubele Stefano, Trabucchi Michele, Bladh Sara, Boyer Martha L, Bressan Alessandro, others . Constraining the thermally pulsing asymptotic giant branch phase with resolved stellar populations in the Large Magellanic Cloud // Monthly Notices of the Royal Astronomical Society. 2020. 498, 3. 3283–3301.

Pastorelli Giada, Marigo Paola, Girardi Léo, Chen Yang, Rubele Stefano, Trabucchi Michele, Aringer Bernhard, Bladh Sara, Bressan Alessandro, Montalbán Josefina, others . Constraining the thermally pulsing asymptotic giant branch phase with resolved stellar populations in the Small Magellanic Cloud // Monthly Notices of the Royal Astronomical Society. 2019. 485, 4. 5666–5692.

Riffel Rogério, Mason Rachel E, Martins Lucimara P, Rodríguez-Ardila Alberto, Ho Luis C, Riffel Rogemar A, Lira Paulina, Martin Omaira Gonzalez, Ruschel-Dutra Daniel, Alonso-Herrero Almudena, others . The stellar spectral features of nearby galaxies in the near infrared: tracers of thermally pulsing asymptotic giant branch stars? // Monthly Notices of the Royal Astronomical Society. 2015. 450, 3. 3069–3079.

Rosenfield Philip, Marigo Paola, Girardi Léo, Dalcanton Julianne J, Bressan Alessandro, Williams Benjamin F, Dolphin Andrew. Evolution of thermally pulsing asymptotic giant branch stars. V. Constraining the mass loss and lifetimes of intermediate-mass, low-metallicity AGB stars // The Astrophysical Journal. 2016. 822, 2. 73.

Sarajedini Ata, Dotter Aaron, Kirkpatrick Allison. DEEP 2MASS PHOTOMETRY OF M67 AND CALIBRATION OF THE MAIN-SEQUENCE J- KS COLOR DIFFERENCE AS AN AGE INDICATOR // The Astrophysical Journal. 2009. 698, 2. 1872.

Schiavon Ricardo P, Faber SM, Castilho Bruno V, Rose James A. Population Synthesis in the Blue. I. Synthesis of the Integrated Spectrum of 47 Tucanae from Its Color-Magnitude Diagram // The Astrophysical Journal. 2002a. 580, 2. 850.

Schiavon Ricardo P, Faber SM, Rose James A, Castilho Bruno V. Population synthesis in the blue. II. The spectroscopic age of 47 Tucanae // The Astrophysical Journal. 2002b. 580, 2. 873.

Schiavon Ricardo P, Rose James A, Courteau Stéphane, MacArthur Lauren A. A library of integrated spectra of galactic globular clusters // The Astrophysical Journal Supplement Series. 2005. 160, 1. 163.

Tang Jing, Bressan Alessandro, Rosenfield Philip, Slemer Alessandra, Marigo Paola, Girardi Léo, Bianchi Luciana. New PARSEC evolutionary tracks of massive stars at low metallicity: testing canonical stellar evolution in nearby star-forming dwarf galaxies // Monthly Notices of the Royal Astronomical Society. 2014. 445, 4. 4287–4305.

Trager SC, Faber SM, Worthey Guy, González J Jesús. The stellar population histories of early-type galaxies. II. Controlling parameters of the stellar populations // The Astronomical Journal. 2000. 120, 1. 165.

Valcin David, Bernal José Luis, Jimenez Raul, Verde Licia, Wandelt Benjamin D. Inferring the age of the universe with globular clusters // Journal of Cosmology and Astroparticle Physics. 2020. 2020, 12. 002.

Vallenari Antonella, Brown Anthony GA, Prusti Timo, De Bruijne Jos HJ, Arenou F, Babusiaux Carine, Biermann Michael, Creevey Orlagh L, Ducourant Christine, Evans Dafydd Wyn, others . Gaia data release 3-summary of the content and survey properties // Astronomy & Astrophysics. 2023. 674. A1.

Vazdekis Alexandre, Salaris Maurizio, Arimoto Nobuo, Rose James A. 47 Tucanae: The Spectroscopic versus Color-Magnitude Diagram Age Discrepancy // The Astrophysical Journal. 2001. 549, 1. 274.

Verro Kristiina, Trager SC, Peletier RF, Lançon A, Arentsen A, Chen Y-P, Coelho PRT, Dries M, Falcón-Barroso J, Gonneau A, others . Modelling simple stellar populations in the near-ultraviolet to near-infrared with the X-shooter Spectral Library (XSL) // Astronomy & Astrophysics. 2022a. 661. A50.

Verro Kristiina, Trager SC, Peletier RF, Lançon A, Gonneau A, Vazdekis A, Prugniel Philippe, Chen Y-P, Coelho PRT, Sánchez-Blázquez P, others . The X-shooter Spectral Library (XSL): Data Release 3 // Astronomy & Astrophysics. 2022b. 660. A34.

Appendices

A Pyhton code for creating the synthetic spectrum

```
for i, params in enumerate(my_params):
    absmag = params[3] - 5 * np.log10(params[5]) + 5 - params[4]
    try:
        spectrum = create_interpolated_spectrum(params[0], params[1],params[2])
        if i == 0:
            totalspectrum = spectrum * 10**(-0.4*absmag)
        if i > 0:
            totalspectrum += spectrum * 10**(-0.4*absmag)
        if i%50==0:
                spectrum2d = np.column_stack((wave,totalspectrum))
                np.savetxt("spectrum2d_"+str(i)+".csv", spectrum2d, delimiter=",")
    except:
        print('star with'+ str(params[0]) + '_' + str(params[1])+ '_'+
        ↪  str(params[2])+'caused an error')
```

Here *my_params* is a zipped list containing the T_{eff}, $\log g$, [Fe/H], apparent magnitude in the G-band, the extinction in the G-band and the distance for each star. The *create_interpolated_spectrum* function creates the spectrum for the stars using the XSL interpolator. After every 50 stars, we save the current total spectrum to be able to check where errors occurred. The try, except statement was added to still create a full total spectrum even when errors occurred due to the IK interpolator for cool giants.

B Comparison between parsec 1.2S and parsec v2.0 isochrone

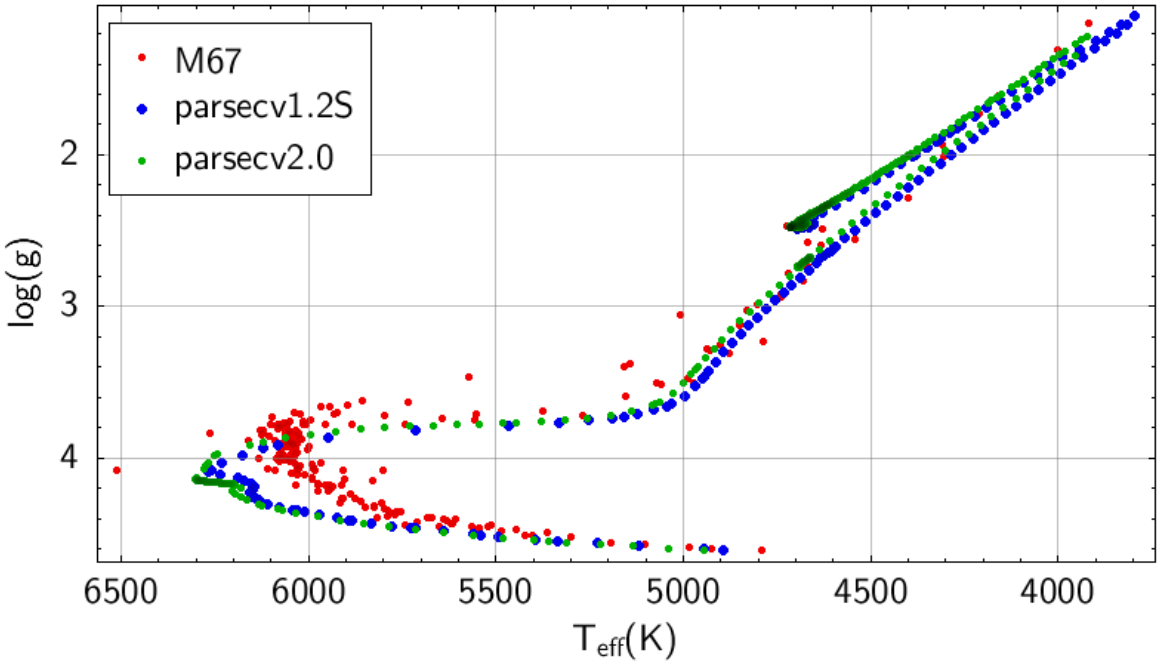

Figure 11: The Kiel diagram of our M67 stars with the parsec v1.2S isochrone and the parsec v2.0 isochrone.